RESEARCH ARTICLE

The Effect of Absorber Stoichiometry on the Stability of Widegap (Ag,Cu)(In,Ga)Se₂ Solar Cells

Patrick Pearson,* Jan Keller, Lars Stolt, Marika Edoff, and Charlotte Platzer Björkman

(Ag,Cu)(In,Ga)Se₂ solar cells with bandgaps of ≈1.45 eV with a large spread in absorber stoichiometry are characterized with the intention of assessing the effect of composition on the stability of the devices. This material is observed to have a poor diffusion length, leading to very strong dependence upon the depletion region width for charge carrier collection. The depletion width is observed to depend strongly upon the stoichiometry value and shrinks significantly after an initial period of dark storage. It is also seen that the depletion width can be varied strongly through light-soaking and dry-heat treatments, with prolonged annealing leading to detrimental contraction and light soaking leading to expansion which increases current collection. The extent of depletion width variation in response to the treatments is also clearly linked to absorber stoichiometry. Consequently, the device performance, particularly the current output, exhibits a stoichiometry dependence and is considerably affected after each round of treatment. Possible causes of this behavior are discussed.

1. Introduction

Cu(In,Ga)Se₂ (CIGS) is an established thin-film photovoltaic material, with record cells reaching efficiencies of 22.6%[1] (or 23.4% with sulfur inclusion).[2] There are still significant improvements to be made, however. The best-performing cells have bandgaps in the region of 1.0–1.2 eV but the optimum value for a single-junction solar cell is 1.34 eV.[3] It would also be advantageous to fabricate high-efficiency widegap CIGS devices to enable the material's use as a top cell in a tandem/multijunction device. To achieve high tandem efficiencies (in the two-terminal configuration), it is estimated that bandgaps of 1.6 and 0.9 eV would be required for top and bottom cells, respectively

(or 1.91, 1.37, and 0.93 eV, for the top, intermediate, and bottom cells in a triple-junction device).[4] Near-maximum theoretical efficiency can be attained for top cells with bandgaps in the region 1.4–1.9 eV in a four-terminal tandem configuration.[5] Furthermore, the increased output voltages and reduced currents of widegap devices allow solar modules with reduced resistive losses and less dead area in monolithic series connections to be manufactured. By increasing the ratio of Ga to In in the material (referred to henceforth as the GGI, $[Ga]/([Ga] + [In])$), the bandgap is also increased, primarily through an energetic increase in the conduction band minimum. However, the open-circuit voltage (V_{OC}) does not increase linearly with the bandgap.[6,7] Currently it seems that the optimal GGI lies in the range of 0.2–0.3 with values in excess of this upper bound leading to deterioration in device performance.[7–9] There are multiple suspected causes for the negative impact of high GGI ratios, including the formation of an unfavorable conduction band offset between the CIGS absorber and cadmium–sulfide (CdS) buffer layer;[10,11] Cu enrichment of grain boundaries (acting either as a region of high recombination or as highly conductive shunt pathways);[12,13] tetragonal distortion of the lattice;[14] or the increase in the energetic depth and density of malign defects.[9,15–17] The incorporation of silver into CIGS, substituting some of the copper atoms, is expected to be beneficial, improving the conduction band offset between the silver-alloyed CIGS (ACIGS) and the commonly used CdS buffer layer.[18] Silver incorporation in CIGS is also observed to increase grain size[19] and reduce the melting point of the alloy, which is expected to reduce the density of defects in the material.[20–22]

With a clear motivation to investigate the incorporation of Ag into CIGS and the realization of high-performance widegap CIGS-based devices, we produced a large series of ACIGS cells, spanning a wide range of compositions.[23] From this work, a compositional window of interest was identified with GGI in the range of 0.66–0.79 and a silver-to-silver-and-copper (AAC) ratio of 0.47–0.67. The upper limit of AAC was chosen to reduce the amount of ordered vacancy compounds (OVCs), forming at the rear of the absorber layer, as it had been concluded that they were detrimental to device performance, acting to block carrier transport. The devices in this region have bandgaps between 1.40 and 1.49 eV and a wide spread in I/III stoichiometry ($I/III = ([Cu] + [Ag])/([In] + [Ga])$). It has been shown that

P. Pearson, J. Keller, L. Stolt, M. Edoff, C. Platzer Björkman
Division of Solar Cell Technology
Department of Material Science
Uppsala University
Box 534, 75121 Uppsala, Sweden
E-mail: patrick.pearson@angstrom.uu.se

The ORCID identification number(s) for the author(s) of this article can be found under https://doi.org/10.1002/pssb.202200104.

OVCs form extensively for largely off-stoichiometric samples with AAC and GGI larger than 0.5.[22] In our previous work, the majority of OVCs were identified to be of the 1:3:5 phase, that is, $(Ag,Cu)(In,Ga)_3Se_5$. This phase has a bandgap approaching 2 eV[23] and is expected to have both conduction and valence band edges significantly below those of the 1:1:2 phase.[24] These factors combined with proximity to the front surface indicate that OVC patches are likely to effectively capture electrons and block carrier collection. It was also observed that Na accumulates in OVCs preferentially to the 1:1:2 phase, which is expected to explain why the presence of OVCs at the rear of the absorber leads to blocking, as the Na reduction in the bulk compromises the $MoSe_2/ACIGS$ interface. In this work we investigate the stability of a smaller subsection of the previous sample set, with a narrower spread in composition and bandgap (1.44–1.47 eV; $0.71 \leq GGI \leq 0.77$; $0.54 \leq AAC \leq 0.63$; $0.79 \leq I/III \leq 0.98$). The narrow spread in AAC and GGI, in comparison with I/III stoichiometry, allows us to focus on the role of the latter parameter in device stability and in the device response to heat and light treatments. By investigating the role of I/III stoichiometry on device stability, we aim also to indirectly probe the effect of OVCs near the front surface of the absorber layer. Overall, six runs each containing four samples (with individual compositions) were analyzed, with some samples excluded due to a high number of dead or shunted cells, leading to a total of 21 samples being characterized.

2. Results

Here we present the external quantum efficiency (EQE) responses and capacitance–voltage (CV) profiles of selected representative cells from across the compositional range, split across two subsections, one detailing the effects of storage and annealing and the other the effects of light soaking (LS). In addition, the evolution of key current–voltage (I–V) performance parameters after treatment, dependent on stoichiometry, is shown for the whole sample set in the storage and annealing section. The second section displays the evolution of V_{OC} with prolonged illumination, showing how the changes induced by LS treatment occur very rapidly. A third section highlights the significance of depletion width in carrier collection. We emphasize now that treatments were performed in sequence, without bringing the samples into a reference state in between (pretests indicate no impact of aging and annealing on the response to LS treatments, while LS is observed to induce permanent doping changes. See Figure S9–S11, Supporting Information). Hence, the differences in performance characteristics discussed in the following sections refer to the difference compared with the values measured after the preceding treatment.

2.1. Effects of Dark Storage and Annealing

Consideration of the EQE responses for four representative cells from across the stoichiometry range (**Figure 1**) indicates that all
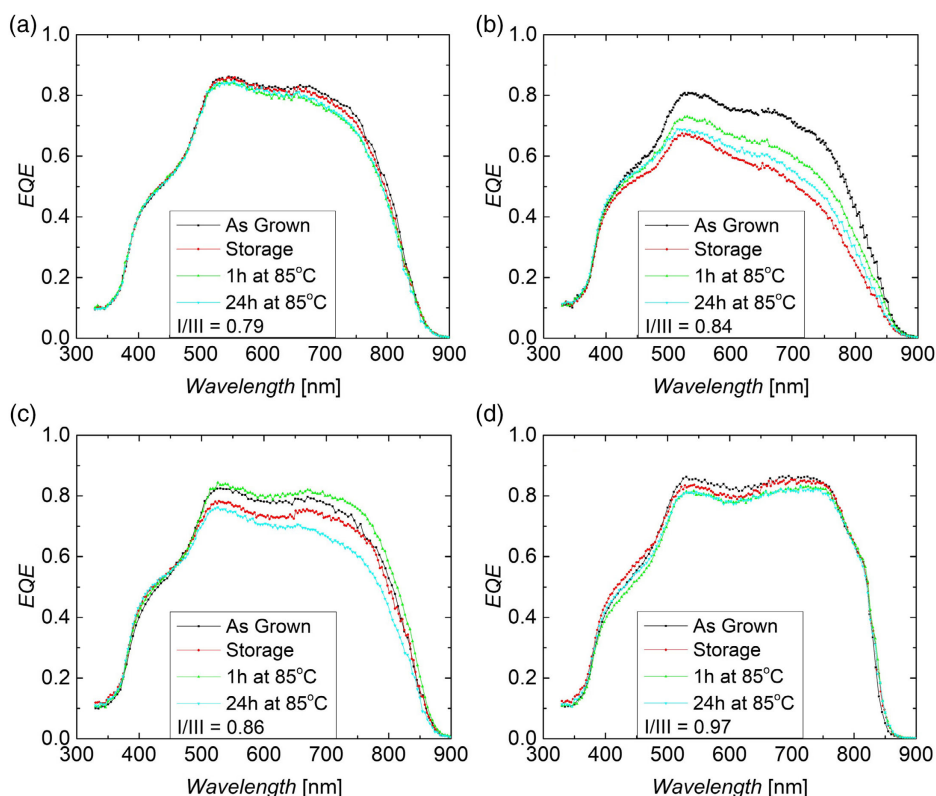

Figure 1. Evolution of EQE response for four different stoichiometries after extended dark storage, a 1 h anneal at 85 °C, and a subsequent 24 h anneal at 85 °C. It can be observed that for extremes of stoichiometry, the treatments have only a small effect on the EQE response, but for samples which are moderately off-stoichiometric, treatment-induced changes are much more severe.

ADVANCED
SCIENCE NEWS
www.advancedsciencenews.com

physica
status
solidi b

www.pss-b.com

cells exhibit a degraded response after extended dark storage, with a resulting loss in J_{SC}. Those cells at the stoichiometric extremes have much less degraded EQE responses. A 1 h anneal at 85 °C is seen to be beneficial for moderately off-stoichiometric devices, with significant improvement in the EQE response across all wavelengths and particularly the long-wavelength regime. Surprisingly, an extended anneal for 24 h at the same temperature was observed to cause a reduction in the EQE response, particularly in the long-wavelength regime, indicating a loss in carrier collection, due either to a reduction in depletion width or to diffusion length.

The effect on the EQE response of storage and heat treatments is mirrored in the doping profiles extracted for the same representative devices (**Figure 2**). A 1 h anneal is observed to significantly expand the depletion width of all cells (all but the least off-stoichiometric sample see increases approaching 100%). A 24 h anneal is then observed to contract the depletion width, particularly for the moderately off-stoichiometric samples, with the reduction exceeding the gain from a single hour in both cases. It was suggested in a previous work[25] that the widegap ACIGS devices have a very poor diffusion length and so exhibit highly depletion-dependent carrier collection. This conclusion is verified by our results, also explaining the minimal shift in the EQE response for samples at the extremes of the stoichiometry range as they are already so heavily depleted, that even considerable contraction or expansion does not significantly affect the collection efficiency in the device, whereas for the narrowly depleted moderately off-stoichiometric samples, minor changes in depletion can cause significant changes in the collection profile. About three months after initial fabrication, a small number of devices were characterized with $C–V$ measurements. A comparison of the depletion widths measured at this time, with regard to the stoichiometry value, indicates that the EQE degradation during the extended dark storage is also likely to stem from the depletion zone contraction, following the responses to annealing (see Figure S1 in the supporting information for more information).

Figure 3a displays the depletion width extracted for each sample, revealing the dependence on I/III. Moreover, through consideration of Figure 3b, it can be seen that those trends observed for the four representative cells are upheld throughout the whole sample set and compositional range. The depletion widths of moderately off-stoichiometric samples are shown to expand after a 1 h anneal, whilst very off- and close-stoichiometric samples do not exhibit significant variation, with the exception of the two most off-stoichiometric samples (I/III = 0.79, 0.81). The subsequent contraction of the depletion width after the 24 h hour anneal also follows such an arch shape. A simple explanation for the dependence of depletion width on stoichiometry, close to stoichiometry, is that there is a decreasing density of group-I vacancies (V_I) toward stoichiometric composition, reducing the net doping. For very off-stoichiometric material, the increase in depletion width is unexpected, as an increase in V_I should increase the acceptor concentration in the material.
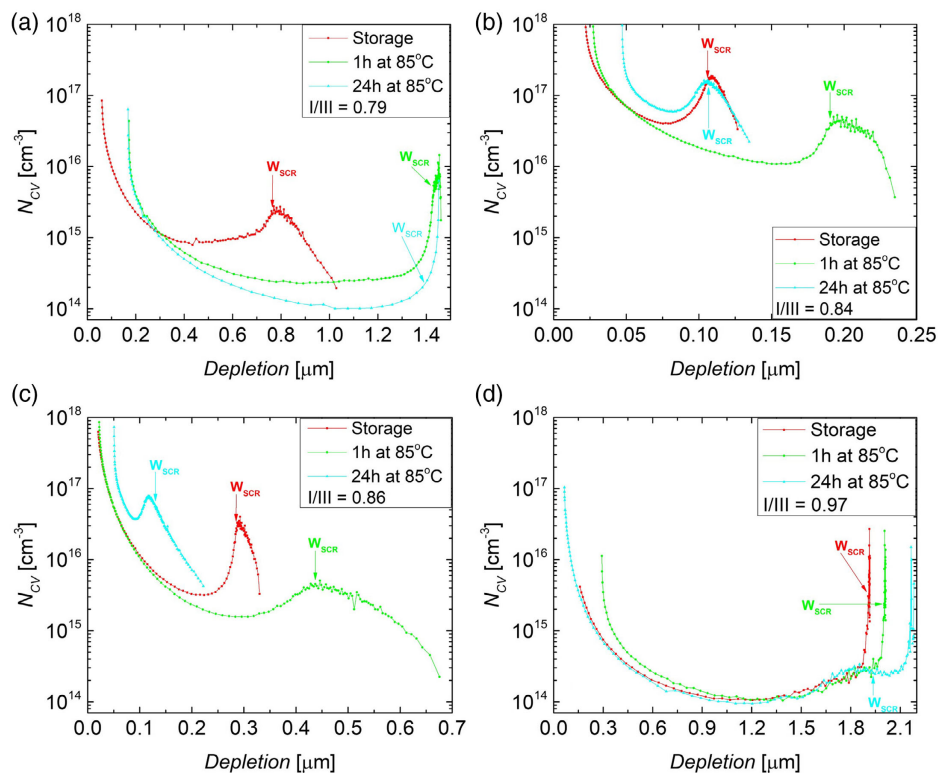

Figure 2. Evolution of the doping profiles of four different stoichiometries after extended dark storage, a 1 h anneal at 85 °C and a 24 h anneal at 85 °C. It can be seen that the shifts observed in the depletion width at zero bias after treatments are related to the shifts in EQE response after treatment (Figure 1), with contraction of the depletion region leading to a reduction in the longer-wavelength EQE response. It can also be seen that devices that are very off-stoichiometric have very wide depletion regions, while close-stoichiometric devices are even fully depleted (note the significant difference in x-scales).
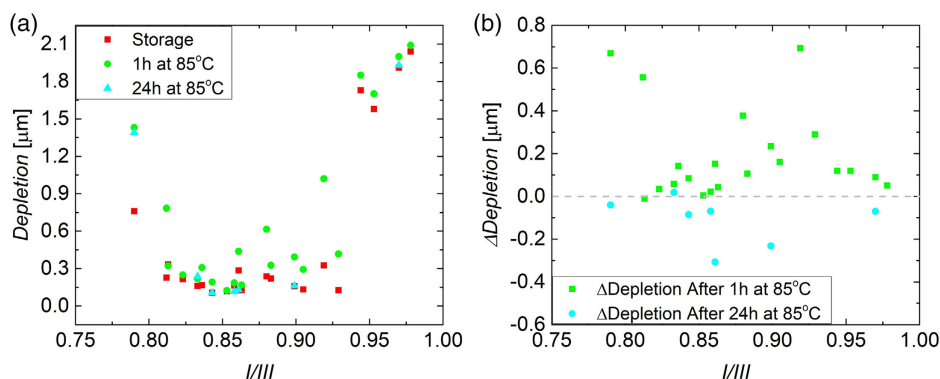
Figure 3. a) The observed dependence of zero-bias depletion width on sample stoichiometry, for all samples, after each round of treatment. Note that for the extremes of the stoichiometry range (I/III $\lesssim$ 0.8, I/III $\gtrsim$ 0.95), depletion is large, reducing significantly in the intermediate region. b) This plot shows how a 1 h anneal leads to a general expansion of the zero-bias depletion width, while the 24 h hour anneal leads to contraction. Both responses follow a similar arch-shaped trend, with relation to stoichiometry.

For such extreme off-stoichiometry, however, the OVC fraction is significant and it is possible that the 1:1:2 phase itself begins to alter. Such dramatic changes to the material system could lead to the observed wide depletion. In addition, as the material becomes increasingly group-I poor, the density of group-III anti-site defects is likely to increase. In/Ga_{Cu} are known donor-type defects in CIGS and the similar radii of In, Ga, and Ag could lead to the formation of In/Ga_{Ag} being more favorable than their Cu counterparts, reducing the net-doping level and expanding the depletion region. This self-compensation is, however, always present in CIGS, so it would be unexpected for the level of self-compensation to become dramatically more pronounced below I/III $\approx$ 0.80.

Turning to the I–V parameters (**Figure 4**), it is seen that there is a slight degradation in V_{OC} after the storage period, with increasing degradation for increasing I/III (Figure 4b). The 1 h anneal is observed to have no clear effect on V_{OC}; however, the 24 h anneal appears to have a beneficial effect on close-stoichiometric samples (I/III $\geq$ 0.90). The response of J_{SC} to each treatment is observed to follow an arch trend, with respect to stoichiometry, with response minima for extremely off- or close-stoichiometric values and the maximum shift at an intermediate value of I/III $\approx$ 0.87 (Figure 4b). This arched dependence on stoichiometry is clearly connected to that of the depletion width seen in Figure 3b. The extended dark storage leads to very significant degradation in J_{SC} (up to 8 mA cm^{-2});
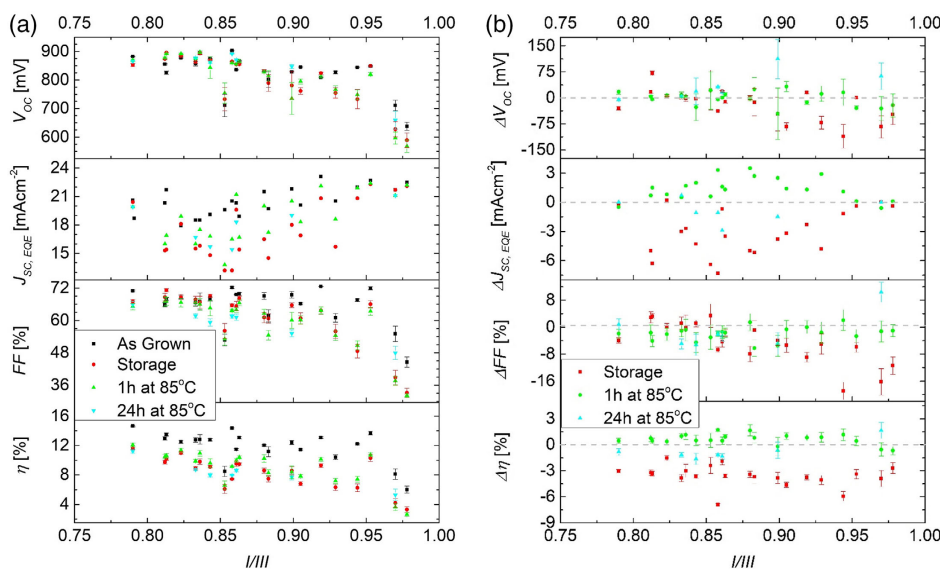

Figure 4. a) Dependence of key I–V performance parameters on stoichiometry for samples as grown, after extended dark storage, and after annealing at 85 °C. b) Dependence of the change in the I–V parameters measured after treatments, on stoichiometry. A clear positive correlation between FF losses over time and stoichiometry can be seen, in addition to a clear stoichiometry-dependent trend for J_{SC} response to treatment, with moderately off-stoichiometric devices being the most responsive. Error bars define the standard error across the samples and data points represent sample averages. As J_{SC} is extracted from single EQE measurements on representative cells, no error bars are given.

however, the short anneal results in partial recovery (gaining up to 4 mA cm^{-2}). In line with the C–V and EQE measurements, the 24 h anneal led instead to further reductions in J_{SC} (peak loss of $\approx$3 mA cm^{-2}). FF was observed to degrade over time, with a clear correlation between stoichiometry and the severity of the degradation. Both anneals led to a slight decrease in FF, but no trend coupling degradation to stoichiometry was observed. It appears that η is led by V_{OC} and FF for close-stoichometric samples, while the off-stoichometric samples are led by variations in J_{SC}. After the storage period, a fairly uniform and significant degradation of $\approx$3% absolute is observed, with slightly greater degradation for samples closer to stoichiometry (presumably stemming from the increased FF and V_{OC} degradation in this compositional region). Following the 1 h anneal, η displays a slight recovery (0.5–1.0%) for all samples with stoichiometry below 0.95, and these close-stoichiometric samples instead exhibit a further degradation of $\approx$1%. After the 24 h anneal, a positive correlation between stoichiometry and recovery can be observed for η, presumably stemming from the similar trend observed for V_{OC}.

2.2. Effects of LS

As with the response to storage and heat treatments, it can be seen in **Figure 5** that devices within the intermediate stoichiometry range have greater responses to LS than those at the extremes of the range, which are affected only very little (the severely off-stoichiometric sample exhibits small gains in

the long-wavelength region, and the close-stoichiometric sample instead exhibits a very minor loss). It can be noted that the extremely off-stoichiometric sample (I/III = 0.79, Figure 5) is subjected to LS, in addition to having previously been annealed for 24 h. This was deemed as acceptable due to the almost non-existent effect of the extended anneal on the device's EQE and C–V responses (the latter in **Figure 6**a). Moreover, the threshold between the extremely and moderately off-stoichiometric effects seems to be at I/III $\approx$ 0.80, so it was necessary to reuse the sample. Interestingly, the sample with I/III = 0.88, which for heating and storage effects can be considered to lie well within the "moderate" range, shows a much reduced response to LS (Figure 5c), compared with the device with I/III = 0.84 (Figure 5b). This may be explained by a comparison of the doping profiles of the two samples (Figure 6b,c). Through consideration of the absorption profile of the material, it can be estimated that $\approx$90% of generation occurs in the first $\approx$1 μm of the absorber material.[25] Due to the poor diffusion length in the material, it can be expected that the carrier collection profile shrinks to zero very quickly for depths outside of the depletion region. Thus, we can expect that for samples with depletion widths $\leq$1 μm, expansion of the depletion region is highly beneficial and will improve collection efficiency significantly; however, further expansion of depletion beyond 1 μm is unlikely to yield significant improvements. With this in mind, we return to the doping profiles of the two samples. Prior to LS, they had depletion widths of $\approx$0.3 and $\approx$0.6 μm for I/III of 0.84 and 0.88, respectively. After
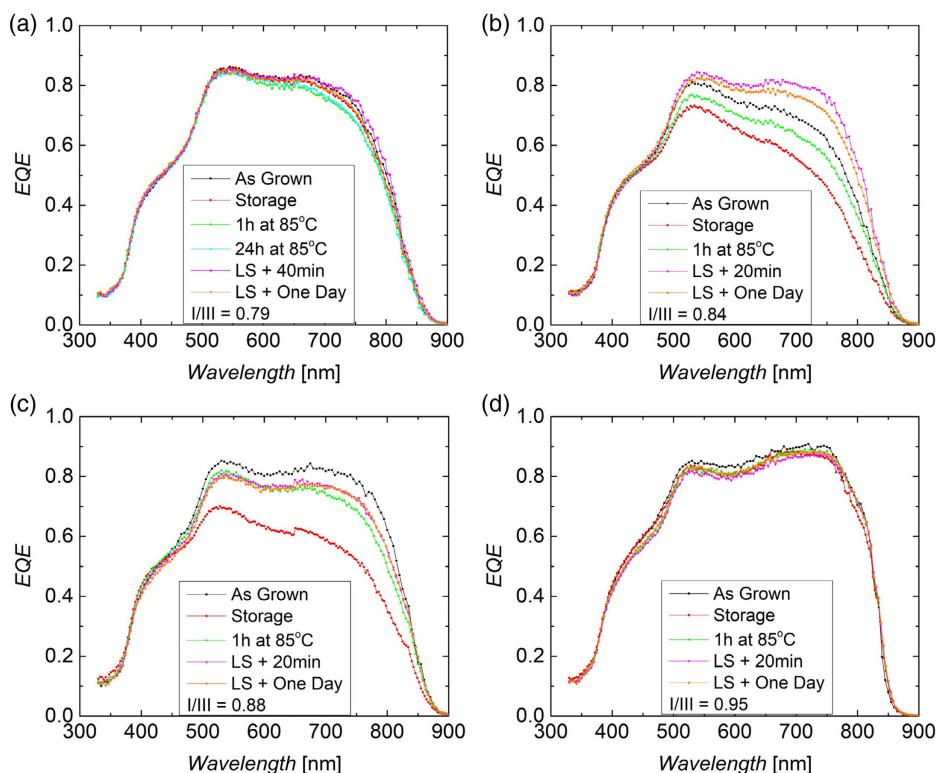

Figure 5. Evolution of EQE response for four different stoichiometries after extended dark storage, a 1 h anneal at 85 °C and 7 h of LS (for I/III = 0.84, 0.88, and 0.95), or 5 h of LS (I/III = 0.79). Again it can be noted that the moderately off-stoichiometric samples respond much more to treatment than those at the extremes of the stoichiometric range.
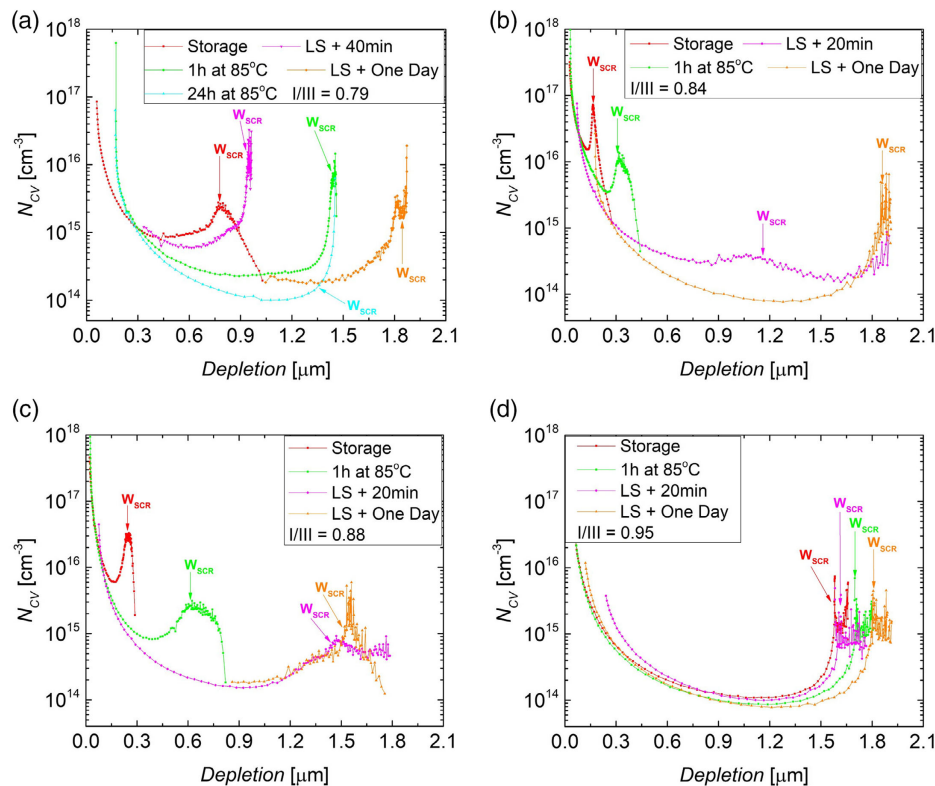
Figure 6. Evolution of the doping profile for four different stoichiometries after extended dark storage, a 1 h anneal at 85 °C, and 7 h of LS (for I/III = 0.84, 0.88, and 0.95) or 5 h of LS (I/III = 0.79). Interestingly it is observed that while the intermediate samples see significant expansion of the depletion region, those at the extremes of the stoichiometric range actually see contraction, particularly the sample with I/III = 0.79.

LS, both samples have depletion regions extending beyond 1 µm. With the improvement limitation we have just established, we see that the sample with I/III = 0.84 had a much greater capacity to improve collection; hence, we observe much greater improvement, despite similar final depletion widths.

It is observed in Figure 6 that for extremely off-stoichiometric devices, the depletion region is significantly contracted (shrinking by more than 0.3 µm), despite also being observed to exhibit improvements in collection (Figure 5). It is suggested that the device is still sufficiently depleted to avoid collection losses from depletion width contraction. Likewise, the close-stoichiometric sample showed a small depletion width contraction but no significant variation in current collection. The samples were measured again, one day after LS. The sample with I/III = 0.84 was observed to lose some collection in the longer wavelengths, while the other sample's responses remained unchanged. This is an unanticipated result, as C–V measurements performed the day after LS reveal that the depletion region of that sample expanded further. Due to the already considerable depletion, we would expect no, or a very slight positive, change to the EQE response. This was the case for the other three samples, wherein each exhibited expansion of the depletion region. The evolution of the depletion width after one day does not appear to show relaxation of the changes induced by LS treatment, as there is no simple reversion of changes (complete or partial).
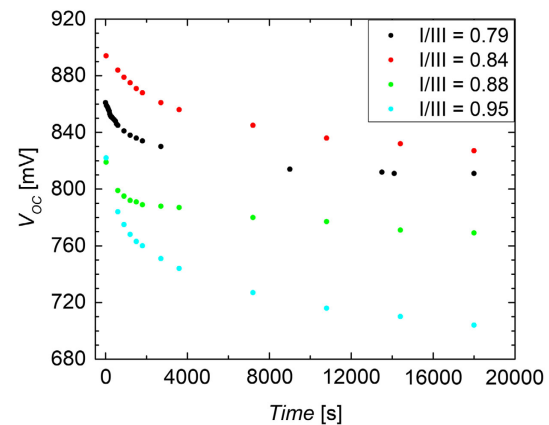

Figure 7. Evolution of the V_{OC} of four devices with different stoichiometries during 5 h of LS. A clear decay in V_{OC} can be observed and we speculate that the main effect occurs up to a time of 4000 s, before temperature effects prevent a final saturation of V_{OC}.

By tracking the evolution of key I–V performance parameters over LS (**Figure 7** and **Table 1**), it was observed that the most significant changes in performance occur within the first 4000 s of LS. V_{OC} is observed to decay steeply within the initial time period, with losses increasing with stoichiometry (35, 50,

Table 1. Evolution of I–V performance parameters over time under AM1.5 illumination. Note the dramatic change in the first 2700 s, followed by more gradual evolution (no measurements were taken near the 4000 s saturation point).

I/III	Time [s]	V_{OC} [mV]	J_{SC} [mA cm^{-2}]	FF [%]	η [%]
0.79	30	859	19.9	67.2	11.5
	2700	830	21.1	66.1	11.6
	18 000	811	21.4	63.3	11.0
0.84	30	894	17.1	56.9	8.7
	2700	861	19.5	67.1	11.3
	18 000	827	21.1	62.0	10.8
0.88	30	819	14.65	59.4	7.1
	2700	788	14.8	60.8	7.1
	18 000	769	15.5	59.9	7.1
0.95	30	822	20.2	63.2	10.5
	2700	751	20.0	61.6	9.3
	18 000	704	20.0	57.7	8.1

75, and 125 mV for I/III of 0.79, 0.84, 0.88, and 0.95, respectively). After this initial decay, it is believed that the gradual degradation in the V_{OC} is due to increasing device temperature (although a Peltier element is used to cool the device during illumination, this system is not perfect, with samples heating from ≈295 to ≈305 K over the illumination period). By performing an I–V measurement 20 min after LS, it was observed that the performance parameters all recovered toward their values at the end of the initial period of rapid change, verifying our suspicion. The highly off-stoichiometric devices (I/III = 0.79 and 0.84) exhibit a steep increase in J_{SC}, which plateaus at the end of the initial 4000 s period, with subsequent low-level gains attributed to temperature effects. The moderately off-stoichiometric sample (I/III = 0.88) shows very minimal improvements in J_{SC} and the close-stoichiometric sample (I/III = 0.95) showed no J_{SC} gains or losses. Unexpectedly, a considerable discrepancy between the EQE and I–V results is noted here, with the EQE response of the extremely off-stoichiometric sample showing only a minor increase and the measured J_{SC} for the intermediate sample I/III = 0.88 being ≈5 mA cm^{-2} greater for EQE than I–V (Table 1). Due to the calibration of the I–V setup, a slight underestimate of J_{SC} is expected for I–V measurements, compared with EQE; however, none of such magnitude was observed previously in this sample set. Interestingly, the discrepancy between the I–V and EQE values of J_{SC} was observed to broaden after each treatment (see Figure S5, Supporting Information); however, an explanation for this cannot be provided. The FF and efficiency of the two moderately off-stoichiometric samples were observed to follow J_{SC} evolution, until the plateau was reached, whereupon V_{OC} reduction could be seen to reduce these figures of merit. The FF and efficiency of the samples at the extremes of the compositional range were observed to be led strongly by V_{OC}.

These results are interesting, as they show a departure from the pattern observed for annealing, of an intermediate "active" stoichiometry region (0.8 ≤ I/III ≤ 0.9), which is highly

responsive to treatment and two unresponsive regions outside the bounds of the intermediate, though the changes in the close-stoichiometric sample mirror those seen after extended dark storage. In the case of V_{OC}, there is a clear direct dependence on stoichiometry, while J_{SC} appears to be more responsive for moderate-to-extremely off-stoichiometric samples and unresponsive for moderately off- to close-stoichiometric samples. This could indicate an alternative mechanism to that driving the changes observed after annealing and storage. The apparent mismatch between J_{SC} gain and depletion evolution for the samples with I/III of 0.79 and 0.88 is attributed to the previously discussed assumption of a maximum beneficial depletion width, beyond which no collection gains are made.

2.3. Effect of Depletion Width on Carrier Collection

Figure 8 shows the extent to which J_{SC} depends on the width of the depletion region, with a clear saturation of improvement once the width of ≈1 μm is reached. It is expected that this depth is needed to absorb the vast majority of incident photons. Indeed this is supported by calculation and absorption measurements made by our group previously for the larger sample set.[25] It can also be seen that by extending the depletion width from 100 to 400 nm, a significant improvement (greater than 50%) in J_{SC} can be delivered. The curves represent J_{SC} values deduced from EQE curves calculated from the generation profile and collection efficiencies, for different depletion width values, assuming a diffusion length of 300 nm, an absorber thickness of 2.0 μm, and a rear-surface recombination velocity of 10^7 cm^{-1}. The collection function was derived from the study by Green et al.[26] and the absorption coefficients were determined using a function adjusted to match previous measurement data (of ungraded representative devices with a bandgap of 1.47 eV); reflection values were also taken from a previously measured
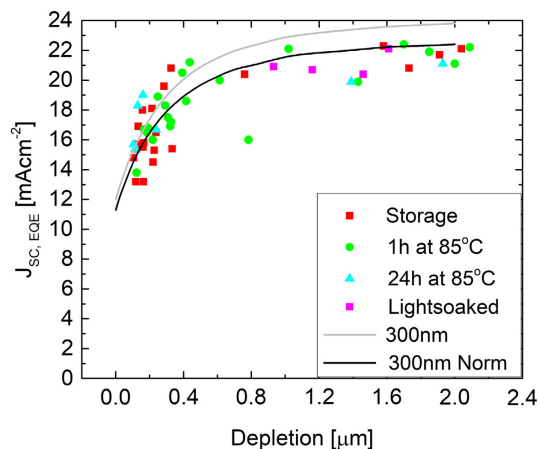

Figure 8. Dependence of J_{SC} (from EQE) on W_{SCR}. The depletion–dependent collection is clear to see from the very steep gradient for 0.0 ≤ depletion width ≤ 0.4 μm and it appears that our earlier estimate of 1.0 μm marking the threshold, beyond which the extension of the depletion region yields little gain, was justified. Calculated EQE responses for similar devices with a bandgap of 1.47 eV and a diffusion length of 300 nm yield a similar trend.

device. The calculated data were normalized to the maximum measured J_{SC} (from EQE) to account for overestimation attributed to differences in reflection and grading between our devices and the reference. It can be seen that the normalized curve is a relatively good fit, confirming that the diffusion length in widegap ACIGS absorbers is indeed rather low (≈300 nm). The absorption data and corresponding simulated EQE spectra can be found in the (Figure S6 and S7, Supporting Information).

3. Discussion

As summarized in **Table 2**, there is a complex interconnection between absorber stoichiometry, applied treatment, and resulting change in I–V parameters. It is, however, clear that the primary driving force for change in performance is the varying doping level/depletion width, but the mechanism that drives this variation is not clear. Moreover, it is unclear how the V_{OC} of moderately and extremely off-stoichiometric devices has relatively small variations, despite considerable increases and decreases in the net doping levels after annealing and storage. Another surprising result is that the effects of a 1 and 24 h anneal are opposing, with the former leading to expanded depletion widths and an improvement in collection, and the latter yielding the reverse both with little-to-no impact on V_{OC}. Figure 8 indicates that the active region of the ACIGS absorbers extends to ≈1 µm, that is, current contribution beyond this depth is negligible. Considering the importance of the first 1000 nm, a layer of several hundred nanometers at the surface could have a significant impact on device performance, but as no such surface layer has been observed for the samples, it is likely that the mechanism driving the effects that we observe is a bulk effect. This suggests

that OVCs do not play a dominant role in what we observe, as they are closely confined to the surface for all but the most off-stoichiometric samples.[23] In order to explain the observed behaviors, we can consider several mechanisms: Mobile ion-driven mechanisms, mechanisms relating to phase stability and segregation, and defect-driven mechanisms. We shall first consider the potential role of mobile ions in our material system.

The possible candidates for ionic diffusion are Na, Cu, and Ag, with all three being highly mobile within the material.[27–30] A selection of samples from across the compositional range were measured with glow-discharge optical emission spectroscopy (GDOES) before and after the 1 h anneal, in order to observe any changes in the elemental distribution (see Figure S2, Supporting Information). The resulting measurements gave no clear indication of ionic redistribution after annealing; however, it is to be noted that this technique provides a laterally integrating depth profile of the elemental distribution, so this result does not rule out diffusion of ions in or out of the grain boundaries (GB) or OVCs. Considering the similar behavior of highly off-stoichiometric and close-stoichiometric samples, it appears that OVCs do not play a key role in the mechanism of depletion width modification that we observe. Consequently, as OVCs have been seen to accumulate large quantities of Na,[23] it also seems unlikely that Na plays a critical role in the processes observed. In order to fully exclude Na migration, devices with Na-free substrates, or substrates containing heavier alkalis will be manufactured in the future, and similar experiments performed.

A possible explanation for the contrasting results of a 1 h and 24 h anneal could be that there is a maximum amount of ion migration that proves to be beneficial for device performance, with an optimum point that, when passed, leads instead to a negative effect on performance. Raghuwanshi, et al. showed that in CIGS, benign GBs are Cu depleted and malign GBs are Cu-rich and contain oxygen.[13] Thus it could be that through annealing, the Cu content of GB is changed and oxygen given a passage into the absorber. Indeed, the devices investigated were not encapsulated, so the ingress of atmospheric elements is a possibility and could have been aggravated through annealing. GDOES data again indicate that this is not the case, with no discernible change in oxygen content after annealing (see Figure S4 and S5, Supporting Information). Deitz et al. also observed clustering of deep defects around certain GBs in ACIGS, with the defect region Cu rich and with sulfur suspected to diffuse from CdS and substitute Se.[31] The long anneal could cause Cu enrichment and diffusion of undesirable elements into GBs. Ag, In, and Ga have very similar ionic radii, so the diffusion of Ag could lead to antisite defects.[19] Although OVCs have been deemed rather unlikely to trigger the depletion width variation, it is to be noted that even for nearly full absorber depletion, highly off-stoichiometric devices never attain EQE spectra as high as those of the close-stoichiometric devices, indicating that there is perhaps a reduction in carrier collection caused by OVCs that operate in parallel with the main observed effects.

We now turn to consider the role of phase stability. Sopiha, et al. indicate that the thermodynamic stability of our compositional window is low, even at 50 °C, indicating that phase separation could begin at our annealing temperature of 85 °C.[32] At such low temperatures, however, this effect would be slow and present on the nanoscale, rather than causing the large

Table 2. Summary of treatment effect on I–V performance parameters for extremely (Ex), moderately- (Mod) and close- (Sto) stoichiometric samples. – indicates that there was no clear trend after treatment, ↑ indicates an improvement, and ↓ indicates a loss. Paired arrows indicate a severe improvement/loss.

	I/III	Dark Storage	1 h Anneal	24 h Anneal	LS
V_{OC}	Ex	–	–	–	↓
	Mod	–	–	–	↓
	Sto	↓	–	↑	↓↓
J_{SC}	Ex	–	–	–	↑
	Mod	↓↓	↑	↓	↑↑
	Sto	–	–	–	–
FF	Ex	–	–	–	↓
	Mod	–	–	–	↑
	Sto	↓↓	–	–	↓
η	Ex	↓	–	↓	↓
	Mod	↓	–	↓	↑
	Sto	↓	–	↓	↓
Depletion	Ex	NA	↑↑	–	↓↓
	Mod	NA	↑↑	↓↓	↑↑
	Sto	NA	↑	–	↓

ADVANCED SCIENCE NEWS
www.advancedsciencenews.com

pssb
physica status solidi b
www.pss-b.com

macroscale changes in performance that we see. Varying GGI and AAC ratios throughout the material would effect the phase separation probability and temperature threshold. However, the kinetics would still be too slow in the investigated temperature range for any phase to degrade so severely and so quickly. Moreover, phase decomposition would be irreversible; however, we observe that partial recovery can be achieved.

Finally we consider the presence of metastable defects, starting with the well-known Lany–Zunger (LZ) model, which explains how the $(V_{Se} - V_{Cu})$ divacancy complex mediates the improvement of device performance after LS and deterioration following dark storage and/or annealing.[33] It is claimed that the divacancy complex has two configurations, one acting as a donor and the other as an acceptor (paired with a deep defect). Illumination enables the conversion of donor-type configurations to acceptor-type configurations, leading to an increase in V_{OC}, while dark annealing leads to relaxation from acceptor- to donor-type configurations. Experimental works using ACIGS devices with much lower Ag and Ga content than here (≤ 0.2 and 0.4, respectively) appear to be consistent with this theory.[34,35] Erslev, et al. investigated LS effects on ACIGS using a broader range of Ag and Ga compositions ($0.16 \leq AAC \leq 0.76$ and $0.29 \leq GGI \leq 0.83$) and also yielded results consistent with LZ theory.[7] Our results are not consistent with the predictions of the LZ theory, at least not those made for ACIGS with much lower Ag and Ga content. It is possible that for much higher Ga and Ag contents than originally considered in the theoretical work, the equilibrium distribution of divacancy configurations is much more acceptor rich (through shifting of the Fermi level), and the barrier to transition to the donor configuration reduces, meaning that upon LS, there is a transition to a donor-type-dominated configuration space. This could then correspond to dark annealing increasing the acceptor-type configuration population, also increasing the deep defect density, and explaining the shrinking depletion width and stable V_{OC} after the prolonged anneal (two parallel yet opposing effects).

Alternatively, we may not have such a defect playing a critical role, but rather another form of the photoactivated barrier, like Czudek, et al. discussed with connection to the persistent photoconductivity effect in CIGS,[36] or metastable defect, such as a DX state (possibly In/Ga$_{Cu}$),[16,37] that is activated or somehow transformed between states through LS and annealing. Indeed, a significant trap state located at $E_V + 0.59$ eV and attributed to Cu$_{In/Ga}$ has been observed in several studies and seen to reduce after annealing, perhaps through reduction of disorder in the material.[31,34] Igalson et al. investigated the dependence of metastable effects on absorber composition and found that for CIGS absorber stoichiometry between 0.8 and ≈ 0.9, the typical metastable defect concentration exceeded 10^{17} cm^{-3}.[38] This range matches our most reactive compositional region. Unfortunately, there is a dearth of theoretical work dealing with the defect nature of high-Ga, high-Ag ACIGS material, so further experimental and theoretical studies are needed for a more comprehensive understanding.

4. Conclusion

To conclude, ACIGS samples with a narrow range of *AAC* and *GGI* values, but with a large spread in I/III stoichiometry, were

characterized using *I–V*, EQE, and *C–V* measurements to investigate their stability with respect to time, heat, and light. It was determined that the key parameter for the material is the doping and corresponding width of the depletion region. Variations in these parameters are seemingly responsible for all other parameter changes that are observed, due mainly to the very low diffusion length in the material. The ease with which the depletion width can be manipulated suggests that treatment-induced performance changes are at least partially reversible, though due to uncertainty surrounding the driving mechanism of the observed changes, it cannot be claimed that these fundamental changes are reversed, in contrast to simply layering opposing effects. Furthermore, as the age, light, and extended annealing treatments led to severe deterioration of output current and voltage, the suitability of this material for real implementation in the field is questionable, unless the degradation can be somehow mitigated. A second issue that became evident in the course of this work is the lack of theoretical investigation into high-Ag and/or high-Ga (A)CIGS devices, particularly with respect to defect theory.

This work leaves several open questions; first among these is what mechanism is acting to change the doping and depletion width after the treatments? The primary candidates are ion migration around GB and/or the presence of an undefined metastable defect state. Second, the symmetry between close- and very off-stoichiometric material (for annealing and storage responses) is surprising, though it does indicate that OVCs are not the culprit. Third, why do the 1 and 24 h anneals have opposite effects (and of similar magnitude)? A fourth point of interest is to identify whether there is in fact a different mechanism mediating the responses to annealing and LS treatments, as perhaps indicated by relating responses to stoichiometry. Finally, the limited response of V_{OC} of off-stoichiometric devices to considerable changes in doping and depletion caused by extended storage and annealing remains unclear. These questions require the support of theoretical studies to answer, in addition to further experiments to probe the defect character of the material.

5. Experimental Section

The devices were characterized by *I–V*, EQE and *C–V* measurements. *I–V* and EQE measurements were performed using home-built setups, the former used an ELH lamp for illumination and a water-cooled Peltier element to keep the cell temperatures at 25 °C. *C–V* measurements were performed with an Agilent 4284A Precision LCR Meter and Keithley 2401 Source Meter. The *C–V* measurement sweep frequency was determined via admittance measurements, using the frequency that brought the phase angle closest to 90° ($\approx$60 kHz, for all devices, see Figure S12 and S13, Supporting Information for example data). Voltage bias was swept from -0.5 V to a value near the individual cell's V_{OC} values (about 0.9 V for most cells). The material permittivity was taken to be 10, as our previous work revealed that a value of 12 was too large.[25] Some cells were also studied with GDOES using a Spectruma Analytik GDA 750 HR system.

Each ACIGS processing run involved four samples, placed such that there was a lateral I/III stoichiometry grading, due to the arrangement of the elemental sources. The I/III variation across the run was $\approx$10%, with much smaller variations in GGI and AAC ($\approx$3% for each). For further details, we refer the reader to the study by Keller et al.[25] The devices were fabricated in January, February, and March of 2021, with initial measurements performed at that time. Subsequent measurements were performed in July 2021 to evaluate the effects of aging on the cells after

roughly half a year of dark storage. After these measurements, all samples underwent a dry anneal at 85 °C for 1 h. Then the samples were divided into two groups, one receiving a 24 h dry anneal at 85 °C and the other being light soaked for 7 h under approximate AM1.5 illumination and cooled via the Peltier element built into the sample stage. One sample, with a stoichiometry value of 0.79, underwent both the 24 h hour anneal and a 5 h LS. It is important to highlight that the treatments were performed in sequence, with no reference state established or referred to (see the supporting information for more details).

Each device comprised a stack of the following layers: soda lime glass (SLG)/Mo/NaF/ACIGS/CdS/i-ZnO/ZnO:Al. The Mo back electrode was sputtered (DC) on the glass substrates and NaF (10–15 nm) was then evaporated on top. No alkali diffusion barrier was used, so Na in-diffusion from the SLG was allowed. The ACIGS films were grown via a three-stage (group-I poor, group-I rich, group-I poor) coevaporation process, the Ag/Cu evaporation rate ratio was kept constant throughout. A higher Ga and lower In rate were applied during the initial absorber growth to facilitate the formation of a back-surface field. All ACIGS films exhibited similar GGI depth profiles and the absorber thickness varied between 2.0 and 2.4 μm. The maximum substrate temperature during the second and third stage was set to 550 °C. No alkali postdeposition treatment was applied. Integral compositions were extracted from crosscalibrated X-Ray fluorescence measurements on bare absorbers located at the outer positions of the deposition zone. After absorber formation, a 50 nm-thick CdS buffer layer was grown by chemical bath deposition. The solar cell stacks were finalized by sputtering i-ZnO (70 nm) and ZnO:Al (150 nm; sheet resistance $\approx 50 \, \Omega \, \square^{-1}$) on top. No antireflective coating was used for any of the cells in this study. Each sample was divided into either 16 cells (each with an area of 0.1 cm^2) or 14 cells (each with an area of 0.05 cm^2).

Supporting Information

Acknowledgements

Conflict of Interest

The authors declare no conflict of interest.

Data Availability Statement

The data that support the findings of this study are available from the corresponding author upon reasonable request.

Keywords

[1] P. Jackson, R. Wuerz, D. Hariskos, E. Lotter, W. Witte, M. Powalla, *Phys. Status Solidi RRL* **2016**, *10*, 583.

[2] M. Nakamura, K. Yamaguchi, Y. Kimoto, Y. Yasaki, T. Kato, H. Sugimoto, *IEEE J. Photovoltaics* **2019**, *9*, 1863.

[3] W. Shockley, H. J. Queisser, *J. Appl. Phys.* **1961**, *32*, 510.

[4] A. S. Brown, M. A. Green, *Physica E* **2002**, *14*, 96.

[5] T. Leijtens, K. A. Bush, R. Prasanna, M. D. McGehee, *Nat. Energy* **2018**, *3*, 828.

[6] M. A. Contreras, L. M. Mansfield, B. Egaas, J. Li, M. Romero, R. Noufi, E. Rudiger-Voigt, W. Mannstadt, *Prog. Photovoltaics* **2012**, *20*, 843.

[7] P. T. Erslev, J. Lee, G. M. Hanket, W. N. Shafarman, J. D. Cohen, *Thin Solid Films* **2011**, *519* 7296.

[8] A. Chikhalkar, M. Goryll, W. Shafarman, R. R. King, in *2019 IEEE 46th Photovoltaic Specialists Conference (PVSC)*, IEEE, Piscataway, NJ **2019**, pp. 2150–2154.

[9] B. Huang, S. Chen, H. Deng, L. Wang, M. Contreras, R. Nou, S. Wei, *IEEE J. Photovoltaics* **2014**, *4*, 477.

[10] J. V. Li, S. Grover, M. A. Contreras, K. Ramanathan, D. Kuciauskas, R. Noufi, *Sol. Energy Mater. Sol. Cells* **2014**, *124* 143.

[11] T. Minemoto, T. Matsui, H. Takakura, Y. Hamakawa, T. Negami, Y. Hashimoto, T. Uenoyama, M. Kitagawa, *Sol. Energy Mater. Sol. Cells* **2001**, *67*, 83.

[12] M. Raghuwanshi, E. Cadel, P. Pareige, S. Duguay, F. Couzinie-Devy, L. Arzel, N. Barreau, *Appl. Phys. Lett.* **2014**, *105*, 013902.

[13] M. Raghuwanshi, R. Wuerz, O. Cojocaru-Mirédin, *Adv. Funct. Mater.* **2020**, *30*, 2001046.

[14] M. Balboul, H. Schock, S. Fayak, A. A. El-Aal, J. Werner, A. Ramadan, *Appl. Phys. A* **2008**, *92*, 557.

[15] G. Hanna, A. Jasenek, U. Rau, H. Schock, *Thin Solid Films* **2001**, *387*, 71.

[16] J. Pohl, K. Albe, *Phys. Rev. B: Condens. Matter Mater. Phys.* **2013**, *87*, 245203.

[17] C. Spindler, F. Babbe, M. H. Wolter, F. Ehré, K. Santhosh, P. Hilgert, F. Werner, S. Siebentritt, *Phys. Rev. Mater.* **2019**, *3*, 090302.

[18] J. Keller, K. V. Sopiha, O. Stolt, L. Stolt, C. Persson, J. J. Scragg, T. Törndahl, M. Edoff, *Prog. Photovoltaics* **2020**, *28*, 237.

[19] C. Wang, D. Zhuang, M. Zhao, Y. Li, L. Dong, H. Wang, J. Wei, Q. Gong, *J. Energy Chem.* **2022**, *66*, 218.

[20] W. Shafarman, C. Thompson, J. Boyle, G. Hanket, P. Erslev, J. David Cohen, In *2010 35th IEEE Photovoltaic Specialists Conf.*, IEEE, Piscataway, NJ **2010**, pp. 000325–000329.

[21] T. Nishimura, A. Doi, J. Chantana, A. Mavlonov, Y. Kawano, T. Minemoto, *Sol. Energy* **2021**, *230*, 509.

[22] H. Simchi, B. E. McCandless, K. Kim, J. H. Boyle, R. W. Birkmire, W. N. Shafarman, *IEEE J. Photovoltaics* **2012**, *2*, 519.

[23] J. Keller, L. Stolt, K. V. Sopiha, J. K. Larsen, L. Riekehr, M. Edoff, *Sol. RRL* **2020**, *4*, 2000508.

[24] A. Sharan, F. P. Sabino, A. Janotti, N. Gaillard, T. Ogitsu, J. B. Varley, *J. Appl. Phys.* **2020**, *127*, 065303.

[25] J. Keller, P. Pearson, N. S. Nilsson, O. Stolt, L. Stolt, M. Edoff, *Sol. RRL* **2021**, *5*, 2100403.

[26] M. A. Green, *Prog. Photovoltaics* **2009**, *17*, 57.

[27] V. Fjallstrom, P. M. Salome, A. Hultqvist, M. Edoff, T. Jarmar, B. G. Aitken, K. Zhang, K. Fuller, C. K. Williams, *IEEE J. Photovoltaics* **2013**, *3*, 1090.

[28] M. Theelen, N. Barreau, V. Hans, H. Steijvers, Z. Vroon, M. Zeman, In *2015 IEEE 42nd Photovoltaic Specialist Conf. (PVSC)*, IEEE, Piscataway, NJ **2015**, pp. 1–6.

[29] J. F. Guillemoles, L. Kronik, D. Cahen, U. Rau, A. Jasenek, H. W. Schock, *J. Phys. Chem. B* **2000**, *104*, 4849.

[30] G. Dagan, T. F. Ciszek, D. Cahen, *Fluid Phase Equilib.* **1992**, *96*, 3013.

[31] J. I. Deitz, P. K. Paul, R. Farshchi, D. Poplavskyy, J. Bailey, A. R. Arehart, D. W. McComb, T. J. Grassman, *Adv. Energy Mater.* **2019**, *9*, 1901612.

[32] K. V. Sopiha, J. K. Larsen, O. Donzel-Gargand, F. Khavari, J. Keller, M. Edoff, C. Platzer-Björkman, C. Persson, J. J. Scragg, *J. Mater. Chem. A* **2020**, *8*, 8740.

[33] S. Lany, A. Zunger, *J. Appl. Phys.* **2006**, *100*, 113725.

[34] A. J. Ferguson, R. Farshchi, P. K. Paul, P. Dippo, J. Bailey, D. Poplavskyy, A. Khanam, F. Tuomisto, A. R. Arehart, D. Kuciauskas, *J. Appl. Phys.* **2020**, *127*, 215702.

[35] A. Ferguson, P. Dippo, D. Kuciauskas, R. Farshchi, J. Bailey, G. Zapalac, D. Poplavskyy, in *2018 IEEE 7th World Conf. on Photovoltaic Energy Conversion (WCPEC)*, IEEE, Piscataway, NJ **2018**, pp. 3918–3922.

[36] A. Czudek, A. Urbaniak, A. Eslam, R. Wuerz, M. Igalson, *IEEE J. Photovoltaics* **2020**, *10*, 1926.

[37] S. Lany, A. Zunger, *Phys. Rev. Lett.* **2008**, *100*, 016401.

[38] M. Igalson, M. Maciaszek, K. Macielak, A. Czudek, M. Edoff, N. Barreau, *Thin Solid Films* **2019**, *669*, 600.